Exsolved Cu–ZnO interfaces for methanol production from CO2 at atmospheric pressure

Journal of Materials Chemistry A

ROYAL SOCIETY OF CHEMISTRY

COMMUNICATION

View Article Online
View Journal

Cite this: DOI: 10.1039/d4ta05812g

Received 19th August 2024
Accepted 24th September 2024

DOI: 10.1039/d4ta05812g

rsc.li/materials-a

Exsolved Cu–ZnO interfaces for methanol production from CO_2 at atmospheric pressure†

Sanaz Soodi,‡[a] Eleonora Calì,‡[b] Shailza Saini,‡[a] William S. Skinner,[c] Alex Martinez Martin,[a] Gwilherm Kerherve,[c] Marco Pietro Mezzapesa,[b] Samir Bensaid,[b] David J. Payne,[d] Melis S. Duyar[a] and Kalliopi Kousi*[a]

An intimate Cu–ZnO interface that allows for the conversion of CO_2 to methanol even at atmospheric pressures was produced using the exsolution method. Detailed characterization and *operando* IR spectroscopy were employed to deconvolute the materials' properties that allow for this to happen.

[a]*School of Chemistry and Chemical Engineering, University of Surrey, Guildford, GU2 7XH, UK. E-mail: k.kousi@surrey.ac.uk*

[b]*Department of Applied Science and Technology, Politecnico di Torino, Corso Duca degli Abruzzi, 24, Turin 10129, Italy*

[c]*Department of Materials, Imperial College London, Exhibition Road, London SW7 2AZ, UK*

[d]*NEOM Education, Research, and Innovation Foundation, Al Khuraybah, Tabuk 49643-9136, Saudi Arabia*

† Electronic supplementary information (ESI) available. See DOI: https://doi.org/10.1039/d4ta05812g

‡ All authors contributed equally.

Kalliopi Kousi

Dr Kalliopi Kousi is a Lecturer at the School of Chemistry and Chemical Engineering at the University of Surrey. Her research background is in Heterogeneous Catalysis and Materials Synthesis and Characterisation. She obtained her degree in Chemistry from the University of Patras, Greece in 2011, where she also got her MRes in 2013 and PhD in 2016. Her current research focuses around nano-engineering of materials for the conversion of greenhouse gases and the production of clean energy. She is also very interested in Science Communication and has been recognised for her work in the EDI space.

Introduction

The UK and EU, along with the rest of the world, have pledged net-zero greenhouse gas emissions by 2050, significantly cutting back on emissions by 2030.[1] There is a wide range of technologies that can help us achieve decarbonisation of our energy supply but in addition to this, we need to capture and utilise the CO_2 still being emitted. The use of hydrogen, coupled with the conversion of that excess CO_2, could result in a ~90% drop in CO_2 emissions associated with the synthesis of chemical feedstocks as compared to current industry practice.[2] Methanol is already acknowledged as a viable bridge to low or net zero emission fuels and chemicals,[3] as it can be used in pure form or as a blend, in internal combustion engines or in direct methanol fuel cells.[4] It is a clean energy resource used to fuel cars, trucks, ships, with the UK spending roughly £150 M to import it yearly.[5] Beyond that, traditional application of methanol in plastics, building blocks, paints, car parts, and construction materials are still of great interest.

Industrially, methanol is currently produced at relatively high temperatures and pressures (200–300 °C, 50–100 bar) over a $Cu/Zn/Al_2O_3$ catalyst using syngas produced through the steam reformation of natural gas.[6] CO_2 hydrogenation to methanol has large-scale application prospects using existing infrastructure and while the conventional industrial methanol process uses syngas that contains CO_2, the majority of the carbon feedstock consists of CO.[7] There are a lot of catalysts that have been studied with various compositions, presenting a range of active metal sites such as Cu, Ni and Pt interfaced with oxides of Ga, In or Zn.[8–13] Although scale up of a CO_2 hydrogenation process has been carried out using these industrial $Cu/Zn/Al_2O_3$ catalysts,[14] switching from a CO to CO_2 feed presents major kinetic and stability challenges for the materials used.[15] Specifically, due to the production of formate as intermediate of CO_2 hydrogenation, Cu catalysts demonstrate a "poisoning" effect from high formate coverages.[16,17] High surface coverages of water which occur during CO_2 hydrogenation also lead to deactivation of Cu catalysts.[18] To improve kinetics of CO_2 hydrogenation, catalyst synthesis

strategies adopting weakening the binding energy of the formate[19] intermediate on the surface or promoting its conversion to methanol can be adopted. Various active sites have been reported for hydrogenation of CO_2 including metallic Cu, oxidized Cu, Zn decorated Cu, and isolated Cu–Zn interfaces[14,20–26] while for the commercial catalyst, there is not a consensus regarding the active interface, and both CuZn bimetallic sites[27,28] and ZnO/Cu[29] interfaces have been proposed as active sites. Creating highly active Cu–Zn interfaces that remain stable under CO_2 hydrogenation conditions (*i.e.* rapid generation of water) and can overcome limitations of Cu–Zn catalysts for CO_2 hydrogenation, are needed to make this process economically favourable.

Exsolution has attracted a lot of interest the last few years as a method to produce stable and highly active catalysts.[30,31] As a disassembly method where nanoparticles are born from within the material, exsolution provides us the opportunity to create systems where the active sites (nanoparticles) have increased interactions with their supports as they are crystallographically aligned with and partly embedded in them.[32] This leads to materials that possess high stability and increased activity as compared to their traditionally prepared analogues and there have already even been some efforts to exsolve copper from different matrixes for different applications.[33–35]

Herein, for the first time, we take advantage of the unique features of the exsolution method to create an intimate relationship between exsolved copper particles and ultra-high dispersed ZnO. We designed a material capable of exsolving Cu surrounded by a pool of Zn and create a powerful interface that allows us to produce methanol from CO_2 at even atmospheric pressures.

Results and discussion

Materials with increased Cu–ZnO interactions and low metal loadings capable of producing methanol at atmospheric pressure

To design a material that would exsolve Cu particles but would also be stable enough to be used in such a challenging application we needed to incorporate an element on the B-site that would keep the material's structure largely intact, hence the choice of Ti. However, the need of also having a labile structure that would promote exsolution led us to the use of A-site and oxygen deficiency.[31] We also decided to use Ca on the A-site as this is also known to facilitate cation mobility and hence enhance exsolution.[35,36] The A-site deficiency is providing the materials with a thermodynamically stable structure after exsolution, which has the promise of withstanding high temperatures and pressures due to this and the embedded nature of the exsolved particles formed.[37] Lastly, due to the oxidation states and coordination environments as well as size of Cu and Zn we designed a material that would be able to incorporate both on the B-site of the perovskite. Taking into consideration the above factors we designed and prepared a $La_{0.5}Ca_{0.4}Cu_{0.1}Zn_{0.1}Ti_{0.8}O_{3-\delta}$ perovskite (Fig. 1a). As observed by the stoichiometry, the material does indeed contain a minimal amount of Cu (~3.5 wt%) as compared to the normally ~50 wt% that is found in traditionally prepared (deposition, precipitation) materials.[38,39] This is because materials prepared by exsolution have demonstrated enhanced activity for various reactions due to the enhanced interface of the nanoparticles with their support.[40]

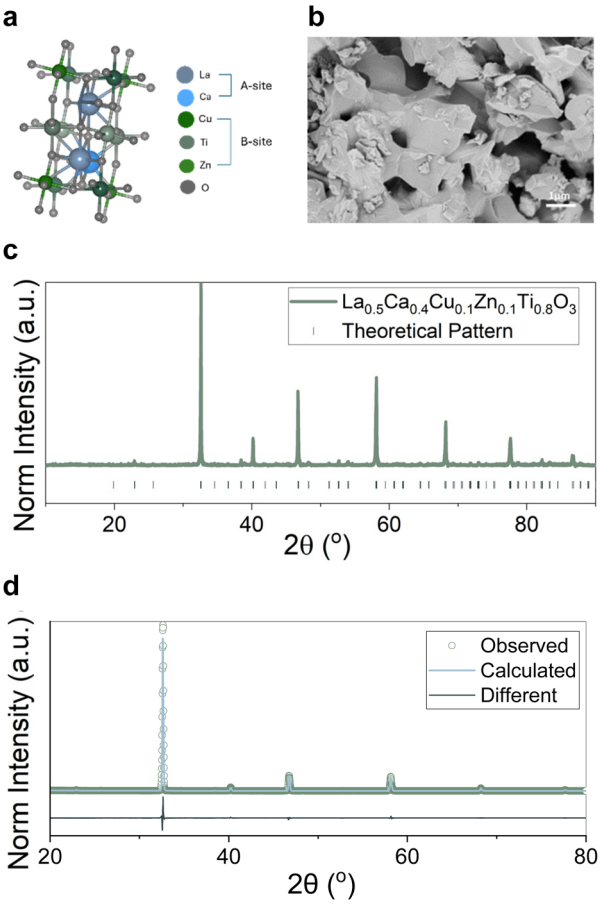

Fig. 1 Synthesizing a system with low substitution of metal and increased Cu–ZnO interactions. (a) Crystal structure of the new material. (b) Microstructure of the as-synthesised catalyst. (c) Room temperature XRD pattern. (d) Rietveld refinement analysis corresponding to a fresh sample shown in (c).

The perovskite was originally synthesised with a solid-state method to ensure control over stoichiometry and was sintered at 1000 °C for 12 h. Fig. 1b demonstrates the microstructure of the as-synthesised catalyst that appears to have a small grain size, a result of the low sintering temperature. The material was indeed of high purity as indicated by X-ray diffraction and Rietveld refinement (Fig. 1c and d) seemingly adopting an orthorhombic crystal structure. The Cu and Zn dopants seem to have been fully incorporated in the structure apparent when compared to the undoped sample (Fig. S1a†) ($La_{0.4}Ca_{0.4}TiO_3$).

After a 10 h reduction at 500 °C, the microstructure of the catalyst remains intact as seen in Fig. 2a, keeping its grain size. X-ray diffraction showed that the sample retained overall its crystallographic properties (Fig. 2b). Two extra peaks appear with the main one at 43.2° (Fig. 2c) and are assigned to metallic Cu particles. Using the Scherrer equation (Fig. S1b†) but also

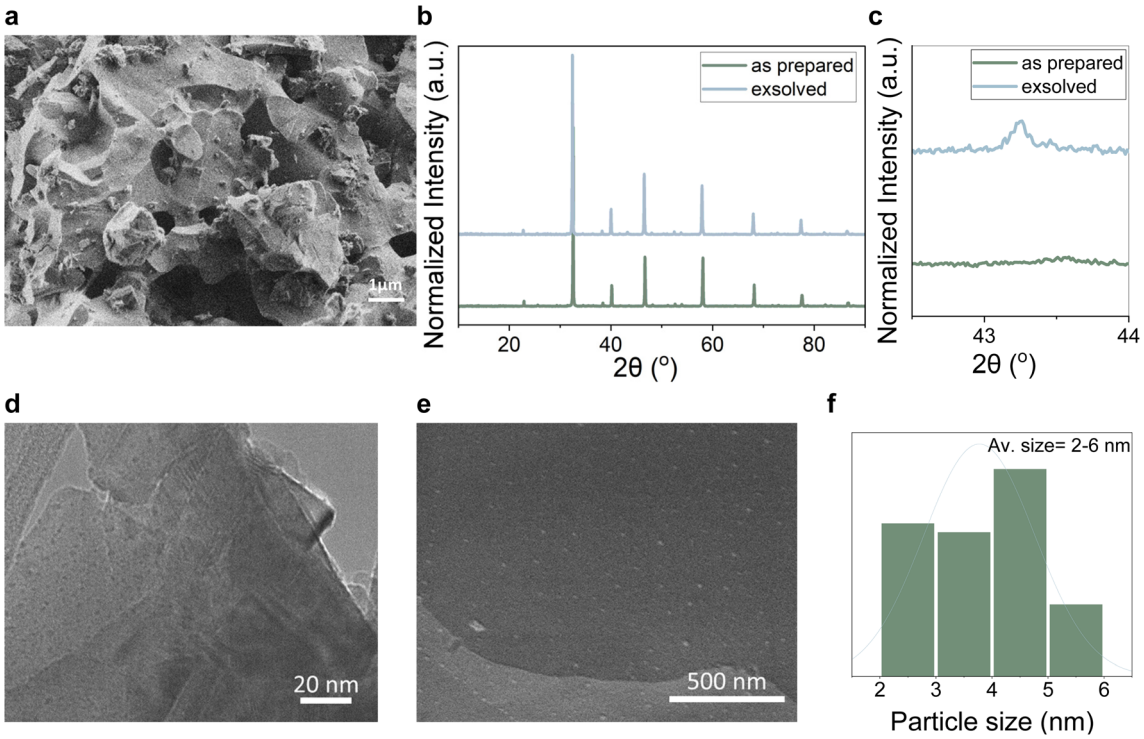

Fig. 2 Activating the exsolved Cu–ZnO interface. (a) Microstructure of the reduced sample. (b) Room temperature XRD pattern for the as sintered and the reduced sample. (c) Close up of the Cu peak. (d) Nanostructure of the reduced sample *via* TEM. (e) Nanostructure of the reduced sample *via* SEM. (f) Particle size distribution obtained *via* ImageJ analysis on the SEM images.

Scanning and Transmission electron microscopies we identify that the metallic copper phase did indeed exsolve in the form of hundreds (~25 000 particles per μm^2) of small ~2–6 nm sized particles (Fig. 2d–f and S2†). We did not pinpoint the presence of any other phase exsolving with any of the analyses conducted, hence we believe that we have created a sample where metallic Cu particles sit within a pool of atomically dispersed Zn ions. This is expected to produce a highly intimate interface between the two phases leading to the production of a highly active new catalyst. The overall calculated amount of Cu exsolved[41] seems to be approximately 10% (~0.32 wt%) (see calculations in ESI†) of the originally doped copper. This value was further corroborated by the refinement of the XRD pattern of the exsolved catalyst. Rietveld refinement showed a 0.3% metallic Cu with high accuracy ($R_{wp} = 5.18$) (Fig. S1c†).

Nevertheless, the newly prepared samples were tested for their activity and selectivity to methanol in the CO_2 hydrogenation reaction at ambient pressure (Fig. 3a and b) at the 200–350 °C temperature range. Our results show that the newly designed material is capable of converting CO_2 to methanol starting at 200 °C. Methanol production keeps increasing throughout the temperature range tested as can be seen in Fig. 3e which is interesting as published literature and theory (Fig. S3†) suggests that methanol production would peak at ~250–280 °C and then decrease while CO would increase with temperature.[42,43] In contrast, here we see an increase in CO production, accompanied by an increase in methanol as well. The TOF values, *i.e.*, the no. of CO_2 molecules hydrogenated per Cu site per sec (s^{-1}) increased significantly from 0.4×10^{-3} at 200 °C to 3.2×10^{-3} at 350 °C (Fig. 3c). This value is ~4 times higher than reported value 0.4×10^{-3} (measured at high p, 3 MPa) for Cu–Zn–Zr catalysts with copper ~45 wt%.[44] This suggests that our catalyst design is of great interest potentially due to the strained nature of the copper sites or the enhanced interaction of Cu with the support *i.e.* ZnO phase.[44] And while the main product is indeed CO, methanol formation at atmospheric pressure is remarkable. Almost the entirety of the published literature that reports methanol production from CO_2 hydrogenation, is mainly under high-pressures (~30–50 bars).[45] In addition,[46] the apparent activation energy (E_a) of CO_2 hydrogenation was also determined (Fig. 3d) and compared to E_a values reported for other catalysts (from 65–86 kJ mol^{-1}) in the literature[17,43] (typically measured at high pressure, 2 MPa) (see Table 1). The E_a for our material was found to be ~36 kJ mol^{-1}, which is significantly lower than the E_a values reported for other catalysts containing much higher copper contents (>50 wt%)[43] and also much lower than its impregnated equivalent (104 kJ mol^{-1}) (Fig. S8c†) (Table 1). Our results indicate that although only a small percentage of the doped copper phase was actually exsolved, indicating that there is still a lot of room for improvement in the material design to be able to drive more copper to the surface of the support, methanol production is possible at atmospheric pressure while using merely 0.3% wt of metal loading, probably owing to the unique interface of the Cu with the Zn containing support. The Cu–Zn interface is known to be crucial for achieving CO_2 conversion to

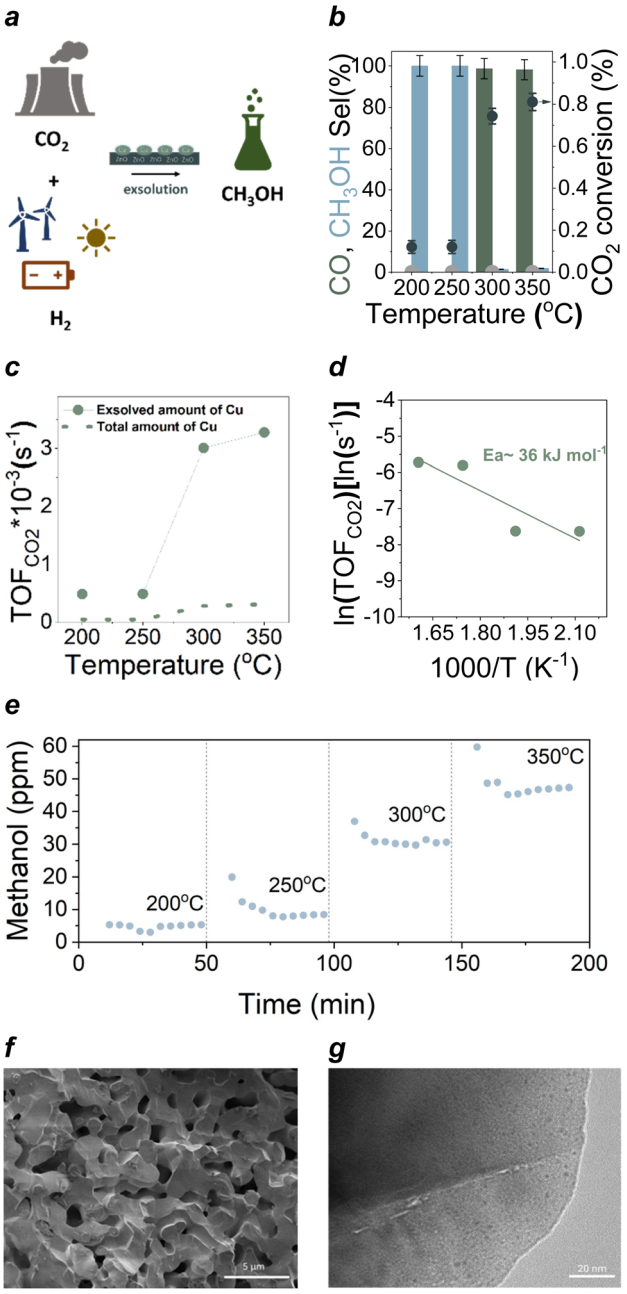

Fig. 3 Producing methanol at atmospheric pressure. (a) Schematic showcasing the use of exsolution in CO_2 to methanol process. (b) Catalytic performance, conditions (P = 1 atm; H_2/CO_2 = 3; GHSV = 7500 mL g cat^{-1} h^{-1}) – grey points represent the support tested under the same conditions. (c) Turn over frequency as the function of temperature. (d) Arrhenius plot of TOF of CO_2 conversion *versus* inverse temperature. (e) Catalytic stability $La_{0.5}Ca_{0.4}Cu_{0.1}Zn_{0.1}Ti_{0.8}O_{3-\delta}$ catalyst under the identical conditions mentioned above. (f) SEM and (g) TEM images after testing.

methanol and the production of methanol at ambient pressure is an indication of the successful interface formation upon exsolution, which complements our characterisation data. Materials characterisation after testing using SEM, TEM, XRD and XPS showed that the micro and nanostructure of the catalyst are intact (Fig. 3f–g and S7†). Specifically, comparison of the Cu 2p and Zn 2p core levels of the exsolved sample measured before catalytic testing (Fig. 4b and d) with those measured afterwards (Fig. S7†) does not indicate any change in chemical state of Cu or Zn, suggesting that the surface is stable under reaction conditions. STEM-EDX elemental maps acquired on several areas of the CuZn exsolved sample after catalytic testing showing dispersed Cu NPs of the same size as the ones found for the reduced sample while XRD showed no additional phases being generated after testing.

Deconvoluting the Cu–ZnO relationship in the exsolved catalysts

In order to better characterise the Cu–ZnO interface and identify the material advancement presented in the exsolved system we employ transmission electron microscopy (Fig. 4a) to look at the surface of the novel material prepared here. STEM-EDX characterization indeed revealed the presence of nanometer-sized nanoparticles, evenly distributed on the surface of the analysed grains, in line with the main characteristic of exsolution. Elemental maps acquired over several regions confirmed the Cu nature of these exsolved nanoparticles, with the other elements composing the novel perovskite material found evenly distributed in the sample. The size distribution of the exsolved nanoparticles was measured to be 2–6 nm, with interparticle distances along the same scale and an intimate Zn distribution possibly surrounding the Cu particles, as partly visible form the EDX elemental distribution map.

To get a deeper understanding of the relationship between copper (Cu) and the support material, X-ray photoelectron spectroscopy (XPS) was employed to measure the sample before and after exsolution. Examination of the XPS data revealed that for both the as-prepared and the exsolved sample the oxidation state and coordination environment of the A-site is essentially unchanged throughout, indicative of A-site stability throughout the redox process (the A-site core level spectra (La 3d, Ca 2p) can be found in the ESI (Fig. S4†), alongside full survey scans along with a table, Table 1, with the measured energies). The signals of La^{3+}, Ca^{2+}, Ti^{4+} and O^{2-} are characteristic of the ones usually reported for a lanthanum calcium titanate. The La 3d and Ca 2p core levels remain essentially unchanged following reduction. Similarly, the Ti 2p core level also remains stable following reduction, aside from the slight change in the relative amounts of Ti^{3+} and Ti^{4+} (Fig. S4†), which could be linked to an increase in the concentration of oxygen vacancies upon reduction. No considerable changes are observed in the O 1s core level following reduction.

The measured Zn 2p (Fig. 4b) and Zn $L_3M_{45}M_{45}$ (Fig. 4c) spectra of the as prepared and exsolved samples suggest a predominance of Zn(II). The Zn $2p_{3/2}$ peak position of the sample before and after reduction (1021.0 eV) matches closely that of ZnO in previous XPS measurements carried out by Biesinger *et al.*[60] The Zn $L_3M_{45}M_{45}$ Auger signal at 989.7 eV has the characteristic shape of Zn(II), but its position is 1.5 eV higher than has previously been observed,[61] corresponding to a modified Auger parameter ($2p_{3/2}$, $L_3M_{45}M_{45}$) of 2011.7, which is 1.5 eV higher than that previously calculated for ZnO.[60,61] This

Table 1 Summary of previous published research of CO_2 hydrogenation to MeOH

Material	Activation energy (kJ mol^{-1})/TOF (s^{-1})	P (bar)	MeOH yield (mmol g_{cat}^{-1} h^{-1})	Byproducts	Ref.
Ru/In_2O_3 (Ru wt% = 2)	E_a not provided/1.77	1	0.12	CO	47
Au–Ni–Ga (Ni wt% = 49)	E_a not provided/3	10	1	CO	48
Au/CeO_2 (Au wt% = 1)	E_a not provided/1.67×10^{-3}	1	0.15	CO, CH_4	49
Au/ZrO_2 (Au wt% = 1)	E_a not provided/2.3×10^{-2}	5	0.66	CO	50
NiGa alloy (ni wt% = 68)	E_a not provided/4.8×10^{-4}	10	0.29	CO	51
NiO–Ga_2O_3/m-SiO_2/Al_2O_3 fibers (Ni/Ga wt% = 7.5)	E_a not provided/9×10^{-4}	1	0.60	CH_4, CO	52[a]
Cu–Al/ZnO rods (Cu wt% = 15)	45.9/4.7×10^{-4}	1	1.9	CO	53
Cu/ZnO/Al_2O_3–La_2O_3 support (Cu wt% = 54)	E_a not provided/5.21×10^{-5}	1	0.60	CO	54
Cu/ZrO_2 (Cu wt% = 5)	E_a not provided/4.5×10^{-2}	1	0.43	CO	55
Cu/ZnO (Cu wt% = 5)	E_a not provided/7.57×10^{-4}	1	0.21	CO	56
Pd–Cu–Zn (Cu wt% = 71)	E_a not provided/8.5×10^{-6}	1	0.29	CO	57
Cu/Zn/Al_2O_3 Commercial	E_a not provided/Cu wt% not provided	1	0.15	CO	58[a]
Cu/ZnO (Cu wt% = 15)	75/7.8×10^{-5}	7	0.11	CO	59
CuZn–LCT (Cu wt% = 0.3)	36/3.2×10^{-3}	1	0.8	CO	This work

[a] Authors of the study conducted CO_2 hydrogenation at $H_2:CO_2$ ratio different of 3 : 1.

could be a result of the difference in chemical environment between Zn(II) as a dopant in the lanthanum calcium titanate perovskite lattice and Zn(II) in ZnO. The considerable similarity between the Zn XPS and Auger spectra of the as prepared and exsolved samples suggests that reduction does not have an observable effect on the chemical state of Zn. In contrast, the measured Cu 2p (Fig. 4d) and Cu $L_3M_{45}M_{45}$ (Fig. 4e) spectra of the as prepared and exsolved samples suggest that all Cu(II) present in the as prepared sample is reduced to either Cu(I) or Cu metal following reduction, owing to the disappearance of the characteristic Cu(II) satellite previously observed for CuO.[60,61] The Cu $2p_{3/2}$ peak position of the sample before reduction (932.8 eV) is approximately 1 eV lower than that typically measured for CuO, lying between the measured binding energies of Cu_2O and CuO.[60–62] Despite considerable overlap with the Ti 2s and Zn Auger peaks, it is still possible to identify the point of highest intensity in the Cu $L_3M_{45}M_{45}$ Auger region, which lies at approximately 915.2 eV. This is 1.3 eV lower than that previously observed for Cu_2O, and 2.6 eV lower than that observed for CuO.[61] We expect that this mismatch between the measured Cu $2p_{3/2}$ and Cu $L_3M_{45}M_{45}$ energies of the as-prepared sample and literature values for Cu_2O and CuO could be explained by either (1) a single chemical state of Cu(II) in the lanthanum calcium titanate perovskite lattice that is distinctly different to that of both Cu_2O and CuO but still presents the characteristic Cu(II) satellite, or (2) a mixture of Cu(I) and Cu(II) states that manifests as a signal lying somewhere between those observed for Cu_2O and CuO. Following reduction, the disappearance of the characteristic Cu(II) satellite feature is accompanied by a 0.3 eV downwards shift in the Cu $2p_{3/2}$ peak position to 932.5 eV, and the apparent emergence of a higher kinetic energy feature in the Cu $L_3M_{45}M_{45}$ Auger region at approximately 918 eV. While it is difficult to be certain of the initial chemical state of Cu in the as prepared sample, we see evidence of reduction in the exsolved sample to either Cu(I) or Cu metal.

The variation in the relative atomic percentage of the different B-site components is plotted in Fig. 4f. In comparing the as-prepared and exsolved samples, a notable decrease in Zn content and corresponding increase in Cu content are observed following reduction, while the overall Ti content remains relatively unchanged. This suggests that some form of exchange may have taken place between Cu ions in the bulk and Zn ions in the near-surface region, with Cu ions preferentially migrating towards the surface which alters their ratio after reduction. Additionally, despite the overall proportion of Ti remaining relatively unchanged, an increase in the relative proportion of Ti^{3+} to Ti^{4+} is observed following reduction. This may be linked to an increase in the concentration of positively charged oxygen vacancy defects upon reduction, which is compensated by reduction of Ti^{4+} to Ti^{3+}.

Mechanistic insights into the process

To investigate the mechanism behind the observed catalytic results, *operando* FTIR spectroscopy was performed on the powder sample pressed into a thin disk for high-temperature gas analysis. A 75% H_2 : 25% CO_2 reagent mixture was introduced in the gas cell over a temperature range between 180–350 °C (7 bar, 15 mL min^{-1}) and outlet signal measured by mass spectrometry (Fig. S5†). Fig. 5 shows the main results obtained while studying the reaction in real time. To investigate intermediate species evolution, the region where formates and carbonates are expected was analysed (~1300–1650 cm^{-1}). Temperature increase resulted in an increase of formate species present between 1560–1600 cm^{-1}.[63] coupled with a decrease of carbonate and carboxylate species associated to TiO_x-based materials (1610–1630 cm^{-1}),[64] as visible in Fig. 5a. This is in line with the already proposed CO_2 hydrogenation mechanism,

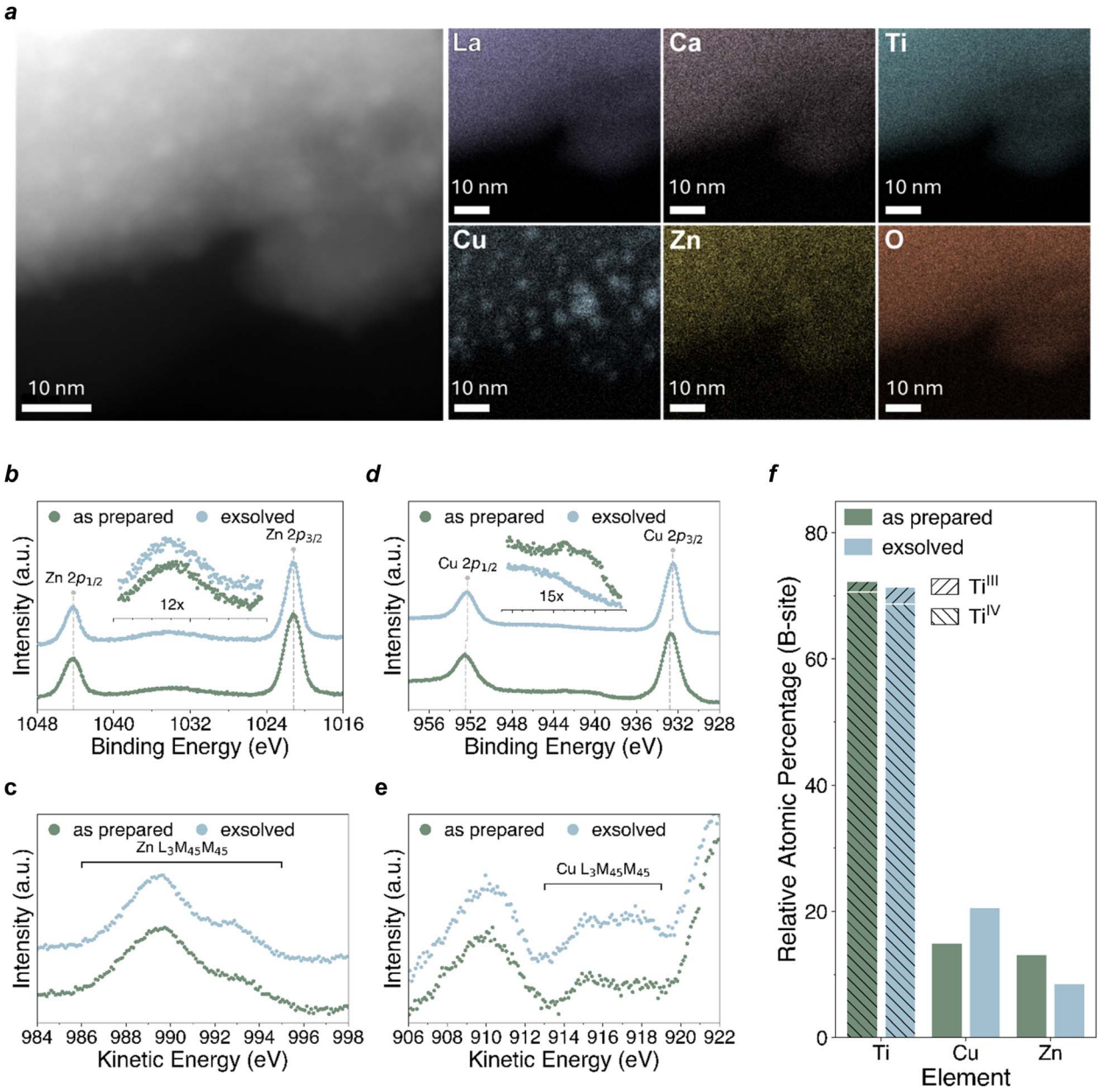

Fig. 4 Deconvoluting the Cu–ZnO relationship. (a) STEM-EDX elemental maps of La, Ca, Ti, Cu, Zn and O acquired on grains of the reduced sample. (b) Zn 2p levels. (c) Zn $L_3M_{4,5}M_{4,5}$. (d) Cu 2p core levels. (e) Cu $L_3M_{4,5}M_{4,5}$ spectra. (f) Relative atomic percentage of the B-site components.

which suggests an initial formation of carbonates at the interface between the support and the metal,[64] Cu in our case. In the literature, this was followed by reduction of the formed carbonates to formates, with consequent CO evolution, and a rapid formate decomposition to surface hydroxyl groups and CO, with production of water.[64] Similarly, here, peaks associated with the presence of formates on Ti^{4+}, Cu^0, and ZnO can be seen at the 1575–1587 cm^{-1} region (Fig. 5b), that would suggest that indeed the mechanism involved in the CO_2 hydrogenation to methanol occurs *via* carbonate–carboxylate consumption and formate evolution over temperature. The support does play an important role in this mechanism, as it has been proposed that CO_2 can be adsorbed over titania surfaces rich in oxygen vacancies, with consequent oxidation of Ti^{3+} to Ti^{4+}, causing CO_2 activation through electron transfer occurring from the Ti in the reduced form to the adsorbed CO_2. To quantitatively verify the CO_2 adsorption properties of our system, CO_2 TPD tests were carried out and the results are reported in the ESI (ESI, Table 2 and Fig. S9†). Three main peaks were identified for our system when running the test up to 500 °C, specifically at ~139 °C, ~232 °C and ~350–360 °C. The first peak can be attributed to CO_2 desorption from weak basic sites on titanate structures, as reported in other works,[65–67] whereas the higher T peaks have been attributed to the presence of medium-strength

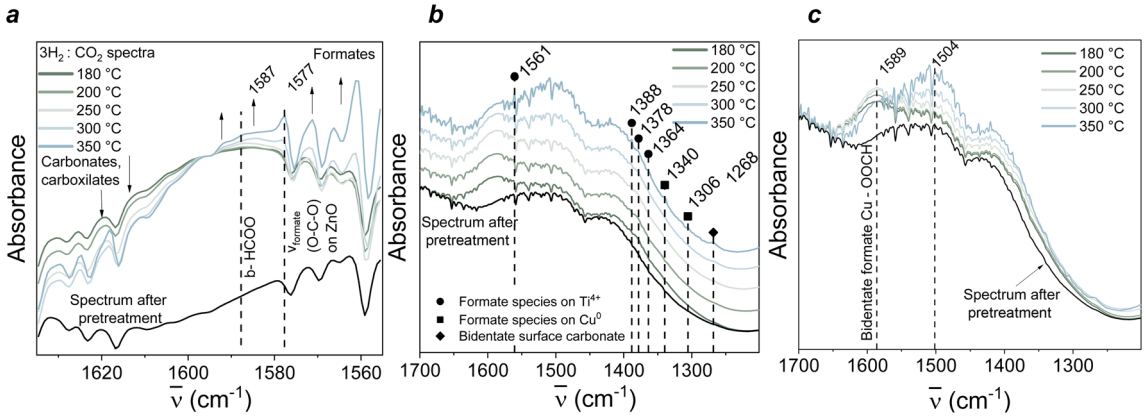

Fig. 5 Mechanistic insights into the process. *Operando* FTIR spectra for the exsolved catalyst showing the evolution of the reaction intermediates in the (a) 1630–1560 cm^{-1} region, (b and c) 1700–1200 cm^{-1} region highlighting the different species evolved during the *operando* CO_2 hydrogenation reaction experiment (75% H_2 : 25% CO_2, 7 bar, 15 mL min^{-1}, NTP).

basic sites from TiO_2 and Cu/TiO_2 structures reduced in the same temperature range as our system,[67,68] and La-based oxides,[54] respectively, with the latter also suggested to increase the adsorption capacity of titanate-based samples.[65] Moreover, the identification of a small amount of Ti^{3+} measured through XPS on the reduced sample after exsolution seems to corroborate this hypothesis, highlighting the role of the high oxygen vacancy concentration in these novel samples for the investigated reaction. A final interesting feature is the broad band observed increasing at ~1500 cm^{-1} when the sample was tested at 300 °C and 350 °C (Fig. 5c), which has been assigned to the ZnO contribution in the CO_2 hydrogenation reaction. Specifically, the intensity of such broad band might be indicative of the amount of defect ionized $V_{O^{\cdot}}$ sites during catalytic reaction, and therefore contributing to the conversion of CO_2 to methanol.[69] This band is already present after N_2 pretreatment in our case which is not surprising, since the analysed sample had undergone extensive reduction to induce exsolution (100% H_2, 500 °C, 10 h), hence also inducing formation of a high extent of V_O. Under *operando* FTIR conditions, photoionization induced by the measurement conditions would cause partial thermal ionization of such mono-ionized oxygen vacancies to $V_{O^{2\cdot}}$, thought responsible for the presence of this broad band. The increase in intensity observed in our case under reaction mixture at 300 and 350 °C compared to what was seen for the exsolved sample pre-testing might suggest formation of $V_{O^{\cdot}}$ donor-type defects by CO_2 during methanol synthesis. The intensity of such band has recently been related to the existence of the metal-oxide (Cu–ZnO) interaction, with higher catalytic activity connected to a higher intensity of the band. This could imply that $Zn^{\delta+}$ sites in partially reduced ZnO under reaction conditions act as CO_2 adsorption sites and reaction intermediates, while the metallic Cu sites interact with H_2 atoms, highlighting the synergy of the active sites present in our exsolved system[69] as also previously reported in various studies.[70,71] Finally, some methane was also detected by MS during the *operando* test. Previous works reported production of methane on pure TiO_2 (011) faceted surfaces through deoxygenation of methoxy groups from Ti cations-V_O vicinity. In our case, a high concentration of oxygen vacancies is produced after nanoparticle exsolution, which could also explain the amount of methane observed.[72]

Post testing analysis verified the presence of nanoscale Cu nanoparticles still present on the support, surrounded by a pool of ZnO (Fig. S6†) which demonstrates the stability of the materials presented here even after submitting them to harsh reaction environments.

Conclusions

There is a wide range of technologies that can help us achieve decarbonisation of our energy supply and achieve our net-zero pledges but in addition to this, we need to utilise the CO_2 still being emitted. CO2 hydrogenation to methanol, a versatile chemical and fuel, can be performed using existing infrastructure but so far material challenges have hindered its wide application. We have designed and prepared a material with Cu exsolved nanoparticles within a pool of ZnO. The material is able to produce methanol starting at 200 °C and atmospheric pressure with only 0.3 wt% of Cu on its surface. We use atmospheric pressure methanol synthesis activity to evaluate the catalytic implications and the success of our strategy to form Cu–ZnO exsolved interfaces. X-ray photoelectron spectroscopy, transition electron microscopy and *operando* infrared spectroscopy indicate that the intimate relationship between the particles and support could be responsible for this. Lastly, although, the material concept demonstrated here requires optimisation in order to drive more Cu sites on the surface of the support, and hence make it even more active, it represents an important advancement in the field of CO_2 hydrogenation reactions. This is also because there is a growing interest in the field of catalysis on non-equilibrium processes, such as forced periodic oscillation[73] or catalytic resonance theory to overcome Sabatier curve rate limitations as well as thermodynamic equilibrium limitations at milder conditions,[74] as well as on dynamic integrated CO_2 capture and conversion processes

where steady-state thermodynamic conversion limitations no longer apply.[75] Hence designing catalysts with low-pressure activity for classically high-pressure reactions such as methanol synthesis holds value beyond the realm of steady-state operation.

Data availability

The research data for this article can be accessed at DOI: https://doi.org/10.15126/surreydata.901036.

Author contributions

Sanaz Soodi data curation; formal analysis; investigation; methodology; writing – original draft; Eleonora Calì data curation; formal analysis; investigation; methodology; writing – original draft; Shailza Saini data curation; formal analysis; investigation; methodology; writing – original draft; William S. Skinner data curation; formal analysis; writing – original draft; Alex Martinez Martin formal analysis; investigation; Gwilherm Kerherve formal analysis; investigation; methodology; Marco Pietro Mezzapesa data curation; formal analysis; Samir Bensaid methodology, funding acquisition; resources; writing – review & editing David J. Payne methodology, funding acquisition; resources; writing – review & editing, Melis S. Duyar methodology, supervision, writing – review & editing Kalliopi Kousi conceptualization; funding acquisition; methodology; project administration; resources; supervision; writing – review & editing.

Conflicts of interest

The authors declare that they have no known competing financial interests or personal relationships that could have appeared to influence the work reported in this paper.

Acknowledgements

The research leading to these results was funded by the School of Chemistry and Chemical Engineering (Chemical and Process Engineering), by the Royal Society RGS\R2\222062, and the Engineering and Physical Science Research Council EP/Y015487/1. E. C. gratefully acknowledges support from the European Union HORIZON-MSCA-2021-PF-01 Marie-Curie Project: 101063146 (MEXCAT).

References

1 United Nations, *Net Zero Coalition*, https://www.un.org/en/climatechange/net-zero-coalition, accessed April 27, 2024.
2 D. Wang, J. Li, W. Meng, Z. Liao, S. Yang, X. Hong, H. Zhou, Y. Yang and G. Li, *J. Cleaner Prod.*, 2023, **412**, 137388.
3 M. Lashgari and S. Soodi, *RSC Adv.*, 2020, **10**, 15072–15078.
4 Q. Shi, Y. He, X. Bai, M. Wang, D. A. Cullen, M. Lucero, X. Zhao, K. L. More, H. Zhou, Z. Feng, Y. Liu and G. Wu, *Energy Environ. Sci.*, 2020, **13**, 3544–3555.
5 UK, https://www.statista.com/statistics/482190/methanol-import-value-in-the-united-kingdom-uk/, accessed April 27, 2024.
6 J. Kotowicz, M. Brzęczek, A. Walewska and K. Szykowska, *Energies*, 2022, **15**, 1480.
7 J. Zuo, K. Chen, J. Zheng, L. Ye and Y. Yuan, *J. CO2 Util.*, 2021, **52**, 101699.
8 Y. Wang, Y. Liu, L. Tan, X. Lin, Y. Fang, X. F. Lu, Y. Hou, G. Zhang and S. Wang, *J. Mater. Chem. A*, 2023, **11**, 26804–26811.
9 A. Gallo, J. L. Snider, D. Sokaras, D. Nordlund, T. Kroll, H. Ogasawara, L. Kovarik, M. S. Duyar and T. F. Jaramillo, *Appl. Catal., B*, 2020, **267**, 118369.
10 S. K. Sharma, B. Paul, R. S. Pal, P. Bhanja, A. Banerjee, C. Samanta and R. Bal, *ACS Appl. Mater. Interfaces*, 2021, **13**, 28201–28213.
11 Z. Shi, M. Pan, X. Wei and D. Wu, *Int. J. Energy Res.*, 2022, **46**, 1285–1298.
12 O. Martin, A. J. Martín, C. Mondelli, S. Mitchell, T. F. Segawa, R. Hauert, C. Drouilly, D. Curulla-Ferré and J. Pérez-Ramírez, *Angew. Chem.*, 2016, **128**, 6369–6373.
13 T. Pinheiro Araújo, C. Mondelli, M. Agrachev, T. Zou, P. O. Willi, K. M. Engel, R. N. Grass, W. J. Stark, O. V. Safonova, G. Jeschke, S. Mitchell and J. Pérez-Ramírez, *Nat. Commun.*, 2022, **13**, 5610.
14 H. Zhang, J. Chen, X. Han, Y. Pan, Z. Hao, S. Tang, X. Zi, Z. Zhang, P. Gao, M. Li, J. Lv and X. Ma, *Ind. Eng. Chem. Res.*, 2024, **63**, 6210–6221.
15 J. Zhong, X. Yang, Z. Wu, B. Liang, Y. Huang and T. Zhang, *Chem. Soc. Rev.*, 2020, **49**, 1385–1413.
16 S. Kuld, M. Thorhauge, H. Falsig, C. F. Elkjær, S. Helveg, I. Chorkendorff and J. Sehested, *Science*, 2016, **352**, 969–974.
17 F. Studt, M. Behrens, E. L. Kunkes, N. Thomas, S. Zander, A. Tarasov, J. Schumann, E. Frei, J. B. Varley, F. Abild-Pedersen, J. K. Nørskov and R. Schlögl, *ChemCatChem*, 2015, **7**, 1105–1111.
18 A. Beck, M. A. Newton, L. G. A. van de Water and J. A. van Bokhoven, *Chem. Rev.*, 2024, **124**, 4543–4678.
19 M. S. Duyar, C. Tsai, J. L. Snider, J. A. Singh, A. Gallo, J. S. Yoo, A. J. Medford, F. Abild-Pedersen, F. Studt, J. Kibsgaard, S. F. Bent, J. K. Nørskov and T. F. Jaramillo, *Angew. Chem., Int. Ed.*, 2018, **57**, 15045–15050.
20 R. Dalebout, L. Barberis, G. Totarella, S. J. Turner, C. La Fontaine, F. M. F. de Groot, X. Carrier, A. M. J. van der Eerden, F. Meirer and P. E. de Jongh, *ACS Catal.*, 2022, **12**, 6628–6639.
21 D. Allam, S. Bennici, L. Limousy and S. Hocine, *C. R. Chim.*, 2019, **22**, 227–237.
22 C. Wu, L. Lin, J. Liu, J. Zhang, F. Zhang, T. Zhou, N. Rui, S. Yao, Y. Deng, F. Yang, W. Xu, J. Luo, Y. Zhao, B. Yan, X.-D. Wen, J. A. Rodriguez and D. Ma, *Nat. Commun.*, 2020, **11**, 5767.
23 J. S. Hayward, The Effects of Secondary Oxides on Copper-Based Catalysts for Green Methanol Synthesis, *ChemCatChem*, 2017, **9**, 1655–1662.
24 Z. Zhong, U. Etim and Y. Song, *Front. Energy Res.*, 2020, **8**, DOI: 10.3389/fenrg.2020.545431.

25 Z. Zhang, X. Chen, J. Kang, Z. Yu, J. Tian, Z. Gong, A. Jia, R. You, K. Qian, S. He, B. Teng, Y. Cui, Y. Wang, W. Zhang and W. Huang, *Nat. Commun.*, 2021, **12**, 4331.
26 M. Lashgari, S. Soodi and P. Zeinalkhani, *J. CO2 Util.*, 2017, **18**, 89–97.
27 K. Stangeland, H. Li and Z. Yu, *Energy, Ecol. Environ.*, 2020, **5**, 272–285.
28 M. Behrens, F. Studt, I. Kasatkin, S. Kühl, M. Hävecker, F. Abild-Pedersen, S. Zander, F. Girgsdies, P. Kurr, B.-L. Kniep, M. Tovar, R. W. Fischer, J. K. Nørskov and R. Schlögl, *Science*, 2012, **336**, 893–897.
29 S. Kattel, P. J. Ramírez, J. G. Chen, J. A. Rodriguez and P. Liu, *Science*, 2017, **355**, 1296–1299.
30 C. Tang, K. Kousi, D. Neagu and I. S. Metcalfe, *Chem.–Eur. J.*, 2021, **27**, 6666–6675.
31 K. Kousi, C. Tang, I. S. Metcalfe and D. Neagu, *Small*, 2021, **17**, 2006479.
32 D. Neagu, J. T. S. Irvine, J. Wang, B. Yildiz, A. K. Opitz, J. Fleig, Y. Wang, J. Liu, L. Shen, F. Ciucci, B. A. Rosen, Y. Xiao, K. Xie, G. Yang, Z. Shao, Y. Zhang, J. Reinke, T. A. Schmauss, S. A. Barnett, R. Maring, V. Kyriakou, U. Mushtaq, M. N. Tsampas, Y. Kim, R. O'Hayre, A. J. Carrillo, T. Ruh, L. Lindenthal, F. Schrenk, C. Rameshan, E. I. Papaioannou, K. Kousi, I. S. Metcalfe, X. Xu and G. Liu, *J. Phys.: Energy*, 2023, **5**, 031501.
33 S. Jo, H. G. Jeong, Y. H. Kim, D. Neagu and J. Myung, *Appl. Catal., B*, 2021, **285**, 119828.
34 L. Fu, J. Zhou, J. Yang, Z. Lian, J. Wang, Y. Cheng and K. Wu, *Appl. Surf. Sci.*, 2020, **511**, 145525.
35 M. Wang, E. I. Papaioannou, I. S. Metcalfe, A. Naden, C. D. Savaniu and J. T. S. Irvine, *Adv. Funct. Mater.*, 2023, **33**, 2302102.
36 J. G. Lee, J.-H. Myung, A. B. Naden, O. S. Jeon, Y. G. Shul and J. T. S. Irvine, *Adv. Energy Mater.*, 2020, **10**, 2070044.
37 D. Neagu, G. Tsekouras, D. N. Miller, H. Ménard and J. T. S. Irvine, *Nat. Chem.*, 2013, **5**, 916–923.
38 D. Kordus, J. Jelic, M. Lopez Luna, N. J. Divins, J. Timoshenko, S. W. Chee, C. Rettenmaier, J. Kröhnert, S. Kühl, A. Trunschke, R. Schlögl, F. Studt and B. Roldan Cuenya, *J. Am. Chem. Soc.*, 2023, **145**, 3016–3030.
39 M. Kourtelesis, K. Kousi and D. I. Kondarides, *Catalysts*, 2020, **10**, 183.
40 M. A. Naeem, P. M. Abdala, A. Armutlulu, S. M. Kim, A. Fedorov and C. R. Müller, *ACS Catal.*, 2020, **10**, 1923–1937.
41 D. Neagu, E. I. Papaioannou, W. K. W. Ramli, D. N. Miller, B. J. Murdoch, H. Ménard, A. Umar, A. J. Barlow, P. J. Cumpson, J. T. S. Irvine and I. S. Metcalfe, *Nat. Commun.*, 2017, **8**, 1855.
42 M. Ren, Y. Zhang, X. Wang and H. Qiu, *Catalysts*, 2022, **12**, 403.
43 R. Ye, L. Ma, J. Mao, X. Wang, X. Hong, A. Gallo, Y. Ma, W. Luo, B. Wang, R. Zhang, M. S. Duyar, Z. Jiang and J. Liu, *Nat. Commun.*, 2024, **15**, 2159.
44 G. Bonura, M. Cordaro, C. Cannilla, F. Arena and F. Frusteri, *Appl. Catal., B*, 2014, **152–153**, 152–161.
45 X. Jiang, X. Nie, X. Guo, C. Song and J. G. Chen, *Chem. Rev.*, 2020, **120**, 7984–8034.
46 A. Prašnikar, A. Pavlišič, F. Ruiz-Zepeda, J. Kovač and B. Likozar, *Ind. Eng. Chem. Res.*, 2019, **58**, 13021–13029.
47 B. Deng, H. Song, Q. Wang, J. Hong, S. Song, Y. Zhang, K. Peng, H. Zhang, T. Kako and J. Ye, *Appl. Catal., B*, 2023, **327**, 122471.
48 M. S. Duyar, A. Gallo, J. L. Snider and T. F. Jaramillo, *J. CO2 Util.*, 2020, **39**, 101151.
49 A. Vourros, I. Garagounis, V. Kyriakou, S. A. C. Carabineiro, F. J. Maldonado-Hódar, G. E. Marnellos and M. Konsolakis, *J. CO2 Util.*, 2017, **19**, 247–256.
50 Y. Hartadi, D. Widmann and R. J. Behm, *ChemSusChem*, 2015, **8**, 456–465.
51 L. F. Rasteiro, M. A. L. S. Rossi, J. M. Assaf and E. M. Assaf, *Catal. Today*, 2021, **381**, 261–271.
52 P. Chen, G. Zhao, Y. Liu and Y. Lu, *Appl. Catal., A*, 2018, **562**, 234–240.
53 S. Du, W. Tang, X. Lu, S. Wang, Y. Guo and P.-X. Gao, *Adv. Mater. Interfaces*, 2018, **5**, 1700730.
54 M. Kourtelesis, K. Kousi and D. I. Kondarides, *Catalysts*, 2020, **10**, 183.
55 S. Kattel, B. Yan, Y. Yang, J. G. Chen and P. Liu, *J. Am. Chem. Soc.*, 2016, **138**, 12440–12450.
56 J. Díez-Ramírez, F. Dorado, A. R. de la Osa, J. L. Valverde and P. Sánchez, *Ind. Eng. Chem. Res.*, 2017, **56**, 1979–1987.
57 J. Díez-Ramírez, J. A. Díaz, P. Sánchez and F. Dorado, *J. CO2 Util.*, 2017, **22**, 71–80.
58 Y.-N. Yang, C.-W. Huang, V.-H. Nguyen and J. C.-S. Wu, *Catal. Commun.*, 2022, **162**, 106373.
59 A. Karelovic and P. Ruiz, *Catal. Sci. Technol.*, 2015, **5**, 869–881.
60 M. C. Biesinger, L. W. M. Lau, A. R. Gerson and R. St. C. Smart, *Appl. Surf. Sci.*, 2010, **257**, 887–898.
61 G. Deroubaix and P. Marcus, *Surf. Interface Anal.*, 1992, **18**, 39–46.
62 S. W. Goh, A. N. Buckley, R. N. Lamb, R. A. Rosenberg and D. Moran, *Geochim. Cosmochim. Acta*, 2006, **70**, 2210–2228.
63 G. Bonura, S. Todaro, L. Frusteri, I. Majchrzak-Kucęba, D. Wawrzyńczak, Z. Pászti, E. Tálas, A. Tompos, L. Ferenc, H. Solt, C. Cannilla and F. Frusteri, *Appl. Catal., B*, 2021, **294**, 120255.
64 L. F. Bobadilla, J. L. Santos, S. Ivanova, J. A. Odriozola and A. Urakawa, *ACS Catal.*, 2018, **8**, 7455–7467.
65 Z. Wang, L. Huang, B. Su, J. Xu, Z. Ding and S. Wang, *Chem.–Eur. J.*, 2020, **26**, 517–523.
66 Y. Ma, J. Liu, M. Chu, J. Yue, Y. Cui and G. Xu, *Catal. Lett.*, 2020, **150**, 1418–1426.
67 H. Deng, X. Zhu, Z. Chen, K. Zhao and G. Cheng, *Carbon Lett.*, 2022, **32**, 1671–1680.
68 C. Zhang, L. Wang, U. J. Etim, Y. Song, O. M. Gazit and Z. Zhong, *J. Catal.*, 2022, **413**, 284–296.
69 S. M. Fehr, K. Nguyen and I. Krossing, *ChemCatChem*, 2022, **14**, e202101500.
70 X. Liu, J. Luo, H. Wang, L. Huang, S. Wang, S. Li, Z. Sun, F. Sun, Z. Jiang, S. Wei, W.-X. Li and J. Lu, *Angew. Chem., Int. Ed.*, 2022, **61**, e202202330.
71 X. Liu, H. Wang and J. Lu, *J. Catal.*, 2024, **436**, 115561.

72 M. Manzoli, A. Chiorino and F. Boccuzzi, *Appl. Catal., B*, 2005, **57**, 201–209.
73 J. Leipold, C. Seidel, D. Nikolic, A. Seidel-Morgenstern and A. Kienle, *Comput. Chem. Eng.*, 2023, **175**, 108285.
74 M. A. Ardagh, T. Birol, Q. Zhang, O. A. Abdelrahman and P. J. Dauenhauer, *Catal. Sci. Technol.*, 2019, **9**, 5058–5076.
75 L.-P. Merkouri, A. I. Paksoy, T. Ramirez Reina and M. S. Duyar, *ACS Catal.*, 2023, **13**, 7230–7242.